Referências Bibliográficas

[1] NOLDIN, J. H. Contribuição ao estudo da cinética de redução de briquetes autoredutores. Dissertação de mestrado, Departamento de Ciência dos Materiais e Metalurgia, Pontifícia Universidade Católica do Rio de Janeiro, Rio de Janeiro, 2002. 1

[2] VIEIRA, C. B.; ARAUJO, F. G. S.; ROSIÉRE, C. A.; SESHADRI, V.; COELHO, L. H. Enfoque geometalúrgico sobre el control de calidad del mineral de hierro en procesos de aglomeración y reducción. *Acero Latinoamericano*, 524:24–33, 2011. 1, 1, 2.1.1

[3] VIEIRA, C. B.; ROSIÈRE, C. A.; SESHADRI, V.; ASSIS, P. S.; COELHO, L. H.; PENA, H. Q. Geometallurgical approach for quality control of iron ores for agglomeration in iron and steel industry. In *International symposium on beneficiation agglomeration and anvironment – ISBAN*, pages 1–7, Bhubaneswar, Índia, 2000. 1

[4] CORNELL, R. M.; SCHWERTMANN, U. *The Iron Oxides: Structure, Properties, Reactions, Occurrences and Uses*. VCH, New York, 2nd edition, 2003. (document), 1, 2.1.1, 2.1.1, 2.2, 2.5

[5] CRIDDLE, A. J.; STANLEY, C. J. *Quantitative Data File for Ore Minerals*. Chapman & Hall, London (UK), 3rd edition, 1993. 1, 2.1.1

[6] PIRARD, E.; LEBICHOT, S. Image analysis of iron oxides under the optical microscope. In *International Congress on Applied Mineralogy: Developments in Science and Technology - (ICAM 2004)*, pages 153–156, Águas de Lindóia, 2004. 1, 2.2

[7] DONSKOI, E.; SUTHERS, S. P.; FRADD, S. B.; YOUNG, J. M.; CAMPBELL, J. J.; RAYNLYN, T. D.; CLOUT, J. M. F. Utilization of optical image analysis and automatic texture classification for iron ore particle characterisation. *Minerals Engineering*, 20:461–471, 2007. 1, 2.2

[8] GOMES, O. D. M.; PACIORNIK, S. Iron ore quantitative characterisation through reflected light-scanning electron co-site microscopy. In *Ninth*

International Congress for Applied Mineralogy, pages 699–702, Carlton: The Australasian Institute of Mining and Metalurgy, 2008. 1, 2.2

[9] GOMES, O. D. M.; PACIORNIK, S. *Scanning Electron Microscopy*, chapter 16. Multimodal Microscopy for Ore Characterization, pages 313–334. InTech (http://www.intechopen.com/books/scanning-electron-microscopy/multimodal-microscopy-for-ore-characterization), 2012. Acesso em: Abril de 2012. 1

[10] VIEIRA, C. B.; ROSIÈRE, C. A.; PENA, E. Q.; SESHADRI, V.; ASSIS, P. S. Avaliação técnica de minérios de ferro para sinterização nas siderúrgicas e minerações brasileiras: uma análise crítica. *Rem: Revista Escola de Minas*, 56 (2):97–102, 2003. 1, 2.1

[11] LIBANEO, C. A. F.; KANEKO, K. M.; COELHO, L. H. T.; PURIFICAÇÃO, E. X. Classificação mineralógica, textural e granulométrica de detalhe de minério de ferro ("pellet feed") e suas implicações geosiderúrgicas. In *III Simpósio Brasileiro de Minério de Ferro. ABM - Associação Brasileira de Metalurgia e Materiais*, pages 70–78, Ouro Preto, Minas Gerais, 2001. 1, 2.2

[12] SANTOS, L. D.; BRANDÃO, P. R. G. LM, SEM and EDS study of microstructure of brazilian iron ores. *Microscopy and Analysis*, 19:17–19, 2005. 1

[13] GRIBBLE, C.; HALL, A. J. *Optical Mineralogy: Principles and practice*. UCL Press, London (UK), 1992. 1, 1

[14] GOLDICH, S. S. Ages of precambrian banded iron-formations. *Economic Geology*, 68 (7):1126–1134, 1973. 2.1

[15] KLEIN, C.; HURLBUT, C. S. *Manual of Mineralogy*. John Wiley & Sons, Inc, New York (NY, USA), 21st edition, 1993. 2.1

[16] LINDENMAYER, Z. G.; LAUX, J. H.; TEIXEIRA, J. B. G. Considerações sobre a origem das formações ferríferas da formação carajás, serra dos carajás. *Revista Brasileira de Geociências*, 31 (1):21–28, 2001. 2.1

[17] VIEIRA, C. B.; ARAUJO, F. G. S; SESHADRI, V.; COELHO, L. H.; ROSIÉRE, C. A. Geometallurgical approach for quality control of iron ores for agglomeration and reduction processes. In *7a Conferencia de Reducción do IAS*, pages 19–36, Campana (Buenos Aires, Argentina), 2009. 2.1

[18] USGS. Mineral commodity summaries. U.S. Department of the Interior. U.S. Geological Survey - (http://minerals.usgs.gov), 2012. Acesso em: Abril de 2012. (document), 2.1, 2.1

[19] IBRAM. Informações e análises da economia mineral brasileira. 6^a Edição. Instituto Brasileiro de Mineração - (http://www.ibram.org.br), 2012. Acesso em: Abril de 2012. (document), 2.1, 2.1, 2.3

[20] DNPM. Sumário mineral. Departamento Nacional de Produção Mineral - (http://www.dnpm.gov.br), 2011. Acesso em: Abril de 2012. (document), 2.1, 2.2

[21] FRICK, M. A. D. Caracterização de minério de ferro por visão computacional. Dissertação de mestrado, Universidade Federal de Santa Maria - UFSM, Rio Grande do Sul, 2008. 2.1

[22] GROSS, G. A. Industrial and genetic models for iron ore in iron formations. In *Mineral Deposit Modeling: Geological Association of Canada*, pages 151–170, Special Paper 40, 1993. 2.1

[23] IABr. Situação atual e principais desafios. Indústria Brasileira do Aço - (http://www.acobrasil.org.br), 2011. Acesso em: Abril de 2012. (document), 2.1, 2.1

[24] ROMERO, T. China: crescimento industrial superior a 16% ao ano pode levar à crise de abastecimento energético. *Inovação Uniemp [online]*, 2 (4):12–15, 2006. 2.1

[25] ROSIÈRE, C. A. Um modelo para a evolução microestrutural dos minérios de ferro doQuadrilátero Ferrífero. Parte II - Trama, textura e anisotropia de susceptibilidade magnética. *Geonomos*, 4 (1):61–75, 1996. 2.1, 2.1.1

[26] ROSIÈRE, C. A.; VIEIRA, C. B.; SESHADRI, V.; CHEMALE JR., F. Classificação genética de minérios de ferro - problemas e vícios - Proposta de uma classificação tipológica para indústria. In *Seminário de Redução de Minério de Ferro da ABM*, pages 295–302, Vitória. Anais, São Paulo, 1997. 2.1

[27] POVEROMO, J. J. Iron ores. In *The Aise Steel Foundation. (Ed.) Ironmaking*, pages 547–550, Pittsburgh, 1999. 2.1

[28] TAKEHARA, L. *Caracterização geometalúrgica dos principais minérios de ferro brasileiros - fração sinter feed.* Tese de doutorado em geociências, Universidade Federal do Rio Grande do Sul, Rio Grande do Sul, 2004. 2.1

[29] VALE. Características estruturais dos finos SECA, SECE, e ALEGRIA que compuseram pilhas de desempenho ruim e excelente na Usiminas. Relatório Interno 1, 22p., Vale, 1998. (document), 2.1, 2.1.1, 2.4

[30] ROSA, M. Segmentação de grãos de hematita em amostras de minério de ferro por análise de imagens de luz polarizada avaliação da qualidade intrínseca de minérios de ferro para uso em altos-fornos. Dissertação mestrado em engenharia de produção, Universidade Federal de Santa Maria, Rio Grande do Sul, 2008. 2.1.1, 2.2, 2.3.5

[31] BARTHELMY, D. Mineralogy database. Webmineral - (http://webmineral.com), 2010. Acesso em: Abril de 2012. (document), 2.1.1, 2.2

[32] KÖNIG, U.; PÖLLMANN , H.; ANGÉLICA, R. S. O refinamento de Rietveld como um método para o controle de qualidade de minérios de ferro. *Rem: Revista Escola de Minas*, 55 (2):111–114, 2002. 2.1.1, 2.2

[33] KARUNAKARAN, C.; SENTHILVELAN, S. Fe2O3-photocatalysis with sunlight and UV light: Oxidation of aniline. *Electrochemistry Communications*, 8 (1):95–101, 2006. 2.1.1

[34] DEER, W. A.; HOWIE, R. A.; ZUSSMAN, J. *Minerais Constituintes das Rochas*. Fundação Calouste Gulbenkian, Lisboa, 2nd edition, 2000. 2.1.1

[35] PACIORNIK, S.; MAURÍCIO, M. H. P. Digital imaging. In *Vander-Voort, G. F. (Ed.). ASM Handbook, v. 9: Metallography and Microstructures*, pages 368–402, Ohio (USA), 2004. 2.2, 2.2, 2.3, 2.3

[36] DOLLEISER, M.; HASHEMI-NEZHAD, S. R. A fully automated optical microscope for analysis of particle tracks in solids. *Nuclear Instruments and Methods in Physics Research B*, 198 (1-2):98–107, 2002. 2.2

[37] HATIBOGLU, C. U.; AKIN, S. A new computerized moving stage for optical microscopes. *Computers & Geosciences*, 30 (5):471–481, 2004. ▷

[38] LEE, S.; GHANTA, S.; KARP, T. Comparative study of retrospective methods to reduce non-uniform illumination effects to bridge coating. *Automation in Construction*, 22:537–544, 2012. ▷

[39] PIRARD, E.; LEBRUN, V.; NIVART, J. F. Optimal acquisition of video images in reflected light microscopy. *Microscopy and Analysis*, 37:19–21, 1999. ▷

[40] YEO, T. T. E.; ONG, S. H.; JAYASOORIAH, SINNIAH, R. Autofocusing for tissue microscopy. *Image and Vision Computing*, 11 (10):629–639, 1993. ▷

[41] SUN, Y.; DUTHALER, S.; NELSON, B. J. Autofocusing in computer microscopy: Selecting the optimal focus algorithm. *Microscopy Research and Technique*, 65:139–149, 2004. ▷

[42] GOLDSMITH, N. T. Deep focus: a digital image processing technique to produce improved focal depth in light microscopy. *Image Anal. Stereol*, 19:163–167, 2000. ▷

[43] VALDECASAS, A. G.; MARSHALL, D.; BECERRA, J. M.; TERRERO, J. J. On the extended depth of focus algorithms for bright field microscopy. *Micron*, 32 (6):559–569, 2001. ▷

[44] YOUNG, I. T. Shading correction: Compensation for illumination and sensor inhomogeneities. In *Current Protocols in Cytometry, J.P. Robinson, et al., Editors., John Wiley and Sons, Inc*, pages 2.11.1–2.11.12, New York (NY, USA), 2000. ▷

[45] MCHUGH, S. White balance. Tutorial about White Balance - (http://www.cambridgeincolour.com/tutorials/white-balance.htm), 2012. Acesso em: Abril de 2012. ▷

[46] BRADLEY, A.; WILDERMOTH, M.; MILLS, P. Virtual microscopy with extended depth of field. In *Proceedings of the International Conference on Digital Image Computing: Techniques and Applications - DICTA*, pages 235–242, Cairns (Australia), 2005. ▷

[47] CARL ZEISS VISION GMBH. KS400. (http://www.zeiss.de), 2001. [software, v. 3.0]. Acesso em: Abril de 2012. 2.2

[48] CARL ZEISS MICROIMAGE GMBH. Axiovision. (http://www.zeiss.de/axiovision), 2010. [software, v.4.8.2]. Acesso em: Abril de 2012. 2.2, 2.3.1.1, 3.2

[49] OLYMPUS SOFT IMAGING SOLUTIONS GMBH. Soft Imaging System (Scandium). (http://www.olympus-sis.com/), 2006. [software, v.3.2]. Acesso em: Abril de 2012. 2.2

[50] CARL ZEISS VISION GMBH. Axioskop 40 pol. clearly superior. (http://earth2geologists.net/Microscopes/documents/Zeiss_Axioscop_Pol_e.pdf), 2012. Acesso em: Abril de 2012. 2.2, 2.2.1, 2.2.1

[51] PIRARD, E. Multispectral imaging of ore minerals in optical microscopy. *Mineralogical Magazine*, 68 (2):323–333, 2004. 2.2

[52] GOMES, O. F. M. *Microscopia Co-Localizada: Novas Possibilidades na Caracterização de Minérios*. Tese de doutorado, Departamento de Ciência dos Materiais e Metalurgia, Pontifícia Universidade Católica do Rio de Janeiro, Rio de Janeiro, 2007. (document), 2.2, 2.3, 2.8, 2.3, ▷, 2.9, 2.3.1.1, 2.3.1.2, 2.3.2, 2.3.5, 2.3.5.3, 2.3.5.3

[53] FERET, F. Routineanalysis of iron ores by x-ray spectrometry. *Spectrochimica Acta Part B: Atomic Spectroscopy*, 37 (4):349–357, 1982. 2.2

[54] GAVIRÍA, J. P.; BOHÉ, A.; PASQUEVICH, A.; PASQUEVICH, D. M. Hematite to magnetite reduction monitored by mössbauer spectroscopy and x-ray diffraction. *Physica B: Condensed Matter*, 389 (1):198–201, 2007. 2.2

[55] COSTA, M. I. JR.; KUNRATH, J. I.; CUNHA, J. B. M.; MORO, J. T.; ARAÚJO, J. H. Mössbauer effect characterization of Brazilian ironores for mining industrial purposes. *Nuclear Instruments and Methods in Physics Research Section B: Beam Interactions with Materials and Atoms*, 76 (1-4):244–245, 1993. 2.2

[56] GANGULY, B.; HUGGINS, F. E.; RAO, K. R. P. M.; HUFFMAN, G. P. Determination of the particle-sizedistribution of iron oxide catalysts from superparamagnetic mössbauer relaxation spectra. *Journal of Catalysis*, 142 (2):552–560, 1993. 2.2

[57] NAYAK, P. K.; DAS, D.; VIJAYAN, V.; SINGH, P. CHAKRAVORTTY, V. 57Fe mössbauer and EDXRF studies on three representative banded iron formations (BIFs) of Orissa, India. *Nuclear Instruments and Methods in Physics Research Section B: Beam Interactions with Materials and Atoms*, 184 (4):649–654, 2001. 2.2

[58] PIRARD, E.; LEBICHOT, S.; KRIER, W. Particle texture analysis using polarized light imaging and grey level intercepts. *International Journal of Mineral Processing*, 84:299–309, 2007. 2.2

[59] DONSKOI, E.; SUTHERS, S. P.; FRADD, S.B.; YOUNG, J. M.; CAMPBELL, J. J.; RAYNLYN, T.D.; CLOUT, J. M. F. Utilization of optical image analysis and automatic texture classification for iron ore particle characterisation. *Minerals Engineering*, 20 (5):461–471, 2007. 2.2

[60] BARBOSA, P. F.; LAGOEIRO, L.; SCHOLZ, R.; GRAÇA, L.; ALVAREZ, G. Electron backscattering diffraction (ebsd) as a tool to evaluate the

topotactic and epitactic growth of minerals: The example of the magnetite and hematite. *Microscopy and Microanalysis*, 17 (2):408–409, 2011. 2.2

[61] BARBOSA, P. F.; LAGOEIRO, L. Crystallographic texture of the magnetite-hematite transformation: Evidence for topotactic relationships in natural samples from quadrilátero ferrífero, brazil. *American Mineralogist*, 95 (1):118–125, 2011. 2.2

[62] NEUMANN, R.; SCHNEIDER, C. L.; ALCOVER-NETO, A. Caracterização tecnológica de minérios. In *Luz, A. B. et al. (Ed.). Tratamento de Minérios. 4. ed*, pages 53–109, Centro de Tecnologia Mineral, Rio de Janeiro, 2004. 2.2

[63] HEILBRONNER, R. Automatic grain boundary detection and grain size analysis using polarization micrographs or orientation images. *Journal of Structural Geology*, 22 (7):969–981, 2000. 2.2

[64] THOMPSON, S.; FUETEN, F.; BOCKUS, D. Mineral identification using artificial neural networks and the rotating polarizer stage. *Computers & Geosciences*, 9 (1):1081–1089, 2001. 2.2

[65] ALVAREZ, J. C.; GOMES, O. F. M.; PACIORNIK, S. Automatic recognition of hematite grains under polarized reflected light microscopy through image analysis. *Minerals Engineering*, 24 (12):1264–1270, 2011. (document), 2.2, 3.1, 3.2, 3.2, 3.3.2, 4.1, 4.1, 4.2, 4.1, 4.2

[66] CASTRO, N.; WIGUM, B. J. Grain size analysis of quartz in potentially alkali-reactive aggregates for concrete: A comparison between image analysis and point-counting. In *10th International Congress for Applied Mineralogy (ICAM)*, pages 103–110, Trondheim, Norway, 2012. 2.2

[67] GOMES, O. D. M.; PACIORNIK, S.; ALVAREZ, J. C. A simple methodology for identifying hematite grains under polarized reflected light microscopy. In *17th International Conference on Systems, Signals and Image Processing - IWSSIP*, pages 428–431, Niterói: EdUFF Editora da Universidade Federal Fluminense, Rio de Janeiro, 2010. (document), 2.3, 2.3.3.2, 3.3.2

[68] HECHT, E. *Optics*. Addison Wesley, New York (NY, USA), 4th edition, 2002. 2.2.1

[69] JR-WORLDWI.DE. Art technic. (http://www.jr-worldwi.de/photo/index.html?polarizer.html), 2012. Acesso em: Junho de 2012. (document), 2.4

[70] WIKIPEDIA. Linearly polarized light. (http://en.wikipedia.org/wiki/Circular_polarizer#Circular_polarizers), 2012. Acesso em: Junho de 2012. (document), 2.5

[71] NAVE, R. Polarization concepts. (http://hyperphysics.phy-astr.gsu.edu/hbase/phyopt/polclas.html), 2012. Acesso em: Junho de 2012. (document), 2.6

[72] DANZ, R.; GRETSCHER, P. C-DIC: a new microscopy method for rational study of phase structures in incident light arrangement. *Thin Solid Films*, 462–463 (2):257–262, 2004. 2.2.1

[73] HIGGINS, M. D. Imaging birefringent minerals without extinction using circularly polarized light. *Canadian Mineralogist*, 48 (1):231–235, 2010. 2.2.1

[74] GOMES, O. F. M. Processamento e análise de imagens aplicada à caracterização automática de materiais. Dissertação de mestrado, Departamento de Ciência dos Materiais e Metalurgia, Pontifícia Universidade Católica do Rio de Janeiro, Rio de Janeiro, 2001. 2.3, 2.3, 2.3.2.1, 2.3.2.2, 2.3.3.1, 2.3.3.2, 2.3.3.2, 2.3.4

[75] VIEIRA, P. R. M.; PACIORNIK, S. Uncertainty evaluation of metallographic measurements by image analysis and thermodynamic modeling. *Materials Characterization*, 47:219–226, 2001. 2.3, 2.3

[76] ALVAREZ, J. C. Uma metodologia para caracterização de sínter de minério de ferro; microscopia digital e análise de imagens. Dissertação de mestrado, Departamento de Ciência dos Materiais e Metalurgia, Pontifícia Universidade Católica do Rio de Janeiro, Rio de Janeiro, 2008. (document), 2.3, 2.3.1.1, 2.12, 2.16

[77] GOMES, O. D. M.; PACIORNIK, S. Caracterização quantitativa de minério de ferro por microcospia co-localizada. *Tecnologia em Metalurgia, Materiais e Mineração*, 6 (2):91–95, 2010. 2.3.1.1

[78] ZITOVÁ , B.; FLUSSER, J. Image registration methods: a survey. *Image and Vision Computing*, 21 (11):977–1000, 2003. 2.3.1.1, 2.3.1.1

[79] BROWN, L. G. A survey of image registration techniques. *ACM Computing Surveys*, 24:325–376, 1992. 2.3.1.1, 2.3.1.1

[80] GOSHTASBY, A. A. *2-D and 3-D Image Registration: for Medical, Remote Sensing, and Industrial Applications*. Wiley-Interscience, New York (NY, USA), 1st edition, 2005. (document), 2.3.1.1, 2.14

[81] HENN, S.; WITSCH, K. Image registration based on multiscale energy information. *Multiscale Modelling Simulation*, 4 (2):584–609, 2005. 2.3.1.1

[82] MAINTZ, J.; VIERGEVER, M. A survey of medical image registration. *Medical Image Analysis*, 2 (1):1–36, 1998. 2.3.1.1

[83] DROSKE, M.; RUMPF, M. A variational approach to nonrigid morphological registration. *SIAM Journal on Applied Mathematics*, 64 (2):668–687, 2004. 2.3.1.1

[84] FISCHER, B.; MODERSITZKI, J. Curvature based image registration. *Journal of Mathematical Imaging and Vision*, 18 (1):81–85, 2003. 2.3.1.1

[85] JANSSENS, G. Improving physical behavior in image registration. In *15th IEEE International Conference on Image Processing (ICIP)*, pages 2952–2955, San Diego (CA, USA), 2008. 2.3.1.1

[86] LOWE, D. G. Distinctive image features from scale-invariant keypoints. *International Journal of Computer Vision*, 60 (2):91–110, 2004. 2.3.1.1

[87] LOWE, D. Object recognition from local scale-invariant features. In *7th IEEE International Conference on Computer Vision*, pages 1150–1157, Kerkyra (Greece), 1999. 2.3.1.1

[88] FIJI-IMAGEJ. Fiji. (http://fiji.sc/wiki/index.php/Fiji), 2012. [software, v.1.45b]. Acesso em: Abril de 2012. 2.3.1.1, 3.2

[89] SUTHERLAND, D.; GOTTLIEB, P. Application of automated quantitative mineralogy in mineral processing. *Minerals Engineering*, 4 (7-11):753–762, 1991. 2.3.1.2

[90] GONZALEZ, R. C.; WOODS, R. E. *Digital Image Processing*. Prentice-Hall, Upper Saddle River (NJ, USA), 3rd edition, 2008. (document), 2.11, 2.3.2, 2.3.2.2, 2.3.2.3, 2.3.3.2, 2.3.5.3, 2.3.5.3

[91] SPRING, K. R. Cameras for digital microscopy. In SLUDER & WOLF, editor, *Methods in Cell Biology*, volume 81: Digital Microscopy, 3rd ed, chapter 10, pages 171–186. Academic Press, San Diego (CA, USA), 2007. 2.3.1.3

[92] TUKEY, J. W. *Exploratory Data Analysis*. Addison-Wesley, Massachusetts (MA, USA), 1st edition, 1977. 2.3.1.3

[93] MARQUES, O.; VIEIRA, H. *Processamento Digital de Imagens*. Brasport, Rio de Janeiro (RJ, Brasil), 1a edition, 1999. 2.3.1.3, 2.3.3.2

[94] PRATT, W. K. *Digital Image Processing*. John Wiley & Sons, New Jersey (NJ, USA), 4th edition, 2007. 2.3.1.3

[95] FACON, J. Processamento e análise de imagens. Pontifícia Universidade Católica do Paraná. Curso de Mestrado em Informática Aplicada - (http://www.ppgia.pucpr.br/ facon), 2005. Acesso em: Abril de 2012. 2.3.2

[96] DESHMUKH, K. S.; SHINDE, G. N. An adaptive color image segmentation. *Electronic Letters on Computer Vision and Image Analysis*, 5 (4):12–23, 2005. 2.3.2

[97] DENG, Y.; MANJUNATH, B. S.; SHIN, H. Color image segmentation. In *IEEE Computer Society Conference on Computer Vision and Pattern Recognition. Vol. 2*, pages 446–451, Fort Collins, (CO, USA), 1999. 2.3.2

[98] TOMITA, F.; YACHIDA, M.; TSUJI, S. Detection of homogeneous regions by structural analysis. In *International Joint Conference on Artificial Intelligence*, pages 2.1–2.12, Stanford (CA, USA), 1973. (i)

[99] WESKA, J. S. A survey of threshold selection techniques. *Computer Graphics and Image Processing*, 7 (2):259–265, 1978. (i)

[100] OTSU, N. A. Threshold selection method from gray-level histograms. *IEEE Transactions on Systems, Man, and Cybernetics*, 9 (1):62–66, 1979. (i), 2.3.2.1

[101] MARR, D.; HILDRETH, E. Theory of edge detection. *Proceedings of the Royal Society of London. Series B, Biological Sciences*, 207 (1167):187–217, 1980. (ii)

[102] CANNY, J. A. Computational approach to edge detection. *IEEE Transactions on Pattern Analysis and Machine Intelligence*, 8 (6):679–698, 1986. (ii), 2.3.2.2, 3.3.2

[103] BRICE, C. R.; FENEMA, C. L. Scene analysis using regions. *Artificial Intelligence*, 1 (3):205–226, 1970. (iii)

[104] FU, K. S. ; MUI, J. K. A survey on image segmentation. *Pattern Recognition*, 13 (1):3–16, 1981. (iii)

[105] BEUCHER, S.; LANTUÉJOUL, C. Use of watersheds in contour detection. In *In International Workshop on Image Processing: Real-time Edge and Motion Detection/Estimation*, pages 2.1–2.12, Rennes (France), 1979. (iv), 2.3.3.2

[106] SERRA, J. *Image Analysis and Mathematical Morphology: Volume 2*. Academic Press, New York (NY, USA), 1st edition, 1988. (iv)

[107] HARALICK, R. M. Statistical and structural approaches to texture. In *Proceedings of the IEEE, Vol. 67, No. 5.*, pages 786–808, 1979. (iv)

[108] PUN, T. Entropic thresholding: A new approach. *Computer Graphics and Image Processing*, 16 (3):210–239, 1981. (iv)

[109] HOROWITZ, S. L.; PAVLIDIS, T. Picture segmentation by a tree transversal algorithm. *Journal of the Association for Computing Machinery*, 23 (2):368–388, 1976. (iv)

[110] HAMMOUCHE, K.; DIAF, M.; SIARRY, P. A multilevel automatic thresholding method based on a genetic algorithm for a fast image segmentation. *Computer Vision and Image Understanding*, 109 (2):163–175, 2008. 2.3.2.1

[111] VALE, G. M.; POZ, A. P. O processo de detecção de bordas de canny: Fundamentos, algoritmos e avaliação experimental. In *Simpósio Brasileiro de Geomática*, pages 292–303, Presidente Prudente, São Paulo, 2002. (ii)

[112] ADAMS, R.; BISCHOF, L. Seeded region growing. *IEEE Transactions on Pattern Analysis and Machine Intelligence*, 16 (6):641–647, 1994. 2.3.2.3

[113] SERRA, J. *Image Analysis and Mathematical Morphology: Volume 1*. Academic Press, New York (NY, USA), 1st edition, 1982. 2.3.3.2

[114] MATHWORKS. Matlab. (http://www.mathworks.com/products/matlab/tryit.html), 2010. [software, v.7.11 (R2010b)]. Acesso em: Maio de 2012. 2.3.3.2, 3.2

[115] DANIELSSON, P. E. Euclidean distance mapping. *Computer Graphics and Image Processing*, 14 (3):227–248, 1980. 2.3.3.2

[116] RUSS, J. C. *The Image Processing Handbook*. CRC Press, Boca Raton (FL, USA), 6th edition, 2011. (document), 2.3.3.2, 2.3.4, 2.3.4, 2.3.4, 2.28, 2.3.5

[117] PACIORNIK, S. Curso de processamento digital de imagens. (http://www.dema.puc-rio.br/cursos/ipdi/index.html), 2012. Acesso em: Maio de 2012. (document), 2.26

[118] GOMES, O. D. M.; PACIORNIK, S. Automatic classification of graphite in cast iron. *Microscopy and Microanalysis*, 11 (4):363–371, 2005. 2.3.4, 2.3.5.2, ▷

[119] GRUM, J.; STURM, R. Computer supported recognition of graphite particle forms in cast iron. *Acta Stereol*, 14 (1):91–96, 1995. 2.3.4, ▷

[120] HOUAISS, I. A. Dicionário eletrônico houaiss da língua portuguesa. Versão 1.05a. Editora Objetiva, 2002. Rio de Janeiro (RJ, Brasil). 2.3.5

[121] THEODORIDIS, S.; KOUTROUMBAS, K. *Pattern Recognition*. Academic Press, Burlington (MA,USA), 4th edition, 2009. 2.3.5, 2.3.5.2

[122] JAIN, A. K.; MURTY, M. N.; FLYNN, P. J. Data clustering: a review. *ACM Computing Surveys*, 31 (3):264–323, 1999. 2.3.5

[123] JAIN, A.K.; DUIN, R.P.W.; MAO J. Statistical pattern recognition: a review. *IEEE Transactions on Pattern analysis and Machine Intelligence*, 22 (1):4–37, 2000. 2.3.5, 2.3.5.1

[124] DUDA, R. O.; HART, P. E.; STORK, D. G. *Pattern Classification*. Wiley, John & Sons, New York (NY, USA), 2nd edition, 2001. 2.3.5.1, 2.3.5.2

[125] BOW, S. T. *Pattern Recognition and Image Preprocessing*. Marcel Dekker, New York (NY, USA), 2nd edition, 2002. 2.3.5.2

A
Artigo da Tese Publicado em Periódico

O método de segmentação Crescimento de Regiões Modificado mostrado neste trabalho rendeu uma publicação no periódico *Minerals Engineering*. Esta publicação serve como requisito parcial para obtenção do título de Doutor pelo Programa de Pós-graduação em Engenharia de Materiais e de Processos Químicos e Metalúrgicos da PUC-Rio. É por isto que esta publicação será anexada à continuação desta página.

Minerals Engineering 24 (2011) 1264–1270

Contents lists available at ScienceDirect

Minerals Engineering

journal homepage: www.elsevier.com/locate/mineng

Automatic recognition of hematite grains under polarized reflected light microscopy through image analysis

Julio Cesar Alvarez Iglesias [a], Otávio da Fonseca Martins Gomes [b,*], Sidnei Paciornik [a]

[a] Dept. of Materials Engineering, Catholic University of Rio de Janeiro (DEMa/PUC-Rio), Rua Marquês de São Vicente, 225, Gávea, 22451-900 Rio de Janeiro, Brazil
[b] CETEM – Centre for Mineral Technology, Av. Pedro Calmon, 900, Ilha da Cidade Universitária, 21941-908 Rio de Janeiro, Brazil

ARTICLE INFO

Article history:
ailable online 5 May 2011

ywords:
n ores
e mineralogy
tificial intelligence
pert systems

ABSTRACT

The recognition of hematite grains is an intermediate task that aids the texture characterization of iron ores. Hematite is a strongly anisotropic mineral. Thus, the combined use of a polarizer and an analyzer in reflected light microscopy (RLM) can be used to obtain images that present sufficient contrast to differentiate grains. The present work proposes a methodology for recognizing hematite grains in images obtained with RLM. Three images per field are acquired in different conditions: without polarization in common bright field arrangement; and with polarization under two symmetrical polarizer/analyzer angles. These images are automatically registered. Then, the hematite grains are recognized through a modified region growing segmentation method based on reflectance and textural information. An optimal value for the polarization angle was determined. The results are promising. The vast majority of grains was correctly recognized. The automatically segmented images were compared to edited versions in which all crystals were correctly discriminated. A statistical comparison of crystal size and shape showed no statistical differences, to within 99% confidence, between automatic and edited segmentation results.

Introduction

The traditional trading of iron ores is based on chemical specifications and particle size distribution. However, recent characterization studies that bring additional information have become important. In fact, porosity, quantitative mineralogy, and texture analysis can contribute to the determination of the iron ores downstream beneficiation operations and subsequent steelmaking process, allowing improvements on both new and existing processes (Vieira et al., 2003; Santos and Brandão, 2005).

It is worth mentioning that the term texture may have different meanings. In Materials Science, texture refers to the distribution of crystallographic orientations of crystallites within polycrystalline materials. On the other hand, in Mineral Technology, texture is sometimes employed as a synonym of fabric to refer to the spatial distribution of different minerals in ore particles or in a rock. In this paper, texture is used in a broad sense. It refers to the spatial distribution of grains within a mineral and to the spatial distribution of different minerals within particles.

Qualitative characterization of iron ores is typically performed by visual examination under the reflected light microscope (RLM). The most common iron-bearing minerals (hematite, magnetite and goethite) can be visually identified on RLM through their distinct reflectances (Criddle and Stanley, 1993).

Automatic image analysis systems are capable of identifying hematite, magnetite and goethite by their colors on suitable RLM images. In recent years some methodologies (Pirard and Lebichot, 2004; Donskoi et al., 2007; Gomes and Paciornik, 2008a,b) were developed to perform mineralogical characterization of iron ores through image analysis systems.

Practically the majority of Brazilian iron ores are of the hematite prevailing type. These ores have a simple mineralogy, generally involving hematite, magnetite, goethite and some gangue minerals, mainly quartz. Nevertheless, they present very diverse microstructures. Different characters of hematite grains, such as lamellar, granular and recrystallized, are found.

Hematite is a strongly anisotropic mineral. It presents bireflectance (Criddle and Stanley, 1993), i.e. its reflectance and consequently its brightness in images changes with different crystal lattice orientations under plane polarized light. This brightness variation is subtle, but it is perceptible to a trained human eye in the RLM.

On the other hand, the combined use of a polarizer and an analyzer in the RLM promotes brightness and color variations due to anisotropy (Gribble and Hall, 1992). This approach can be used to obtain images that present sufficient contrast to

* Corresponding author. Tel.: +55 21 3865 7266; fax: +55 21 2290 4286.
E-mail addresses: julioc.alvarez@gmail.com (J.C.A. Iglesias), ogomes@gmail.com (O.F.M. Gomes), sidnei@puc-rio.br (S. Paciornik).

0892-6875/$ - see front matter © 2011 Elsevier Ltd. All rights reserved.
doi:10.1016/j.mineng.2011.04.015

differentiate grains. Pirard et al. (2007) developed an image processing methodology to detect hematite grain boundaries in which a set of seven images per field is acquired rotating the polarizer by short steps.

The present paper proposes a new approach to perform automatic recognition of hematite grains in images obtained with the RLM. Both polarized and traditional bright field images are combined in an image acquisition, processing and analysis routine that allows discriminating hematite from other phases and detecting the boundaries between hematite crystals. Several polarizer/analyzer setups were tested and optimal discrimination conditions were identified. The count, size and shape of the detected crystals was then automatically obtained and compared to results from manual discrimination for accuracy check.

2. Methodology

2.1. Image acquisition

A motorized and computer controlled RLM with a digital camera (RGB, 24 bits, 1300 × 1030 pixels) was employed to acquire images from polished cross-sections of iron ore samples. Five different fields were selected for their content of hematite regions.

Three images per field were acquired:

- A bright field (BF) RGB *mineralogical image* obtained without polarized light (Fig. 1a).
- Two polarized light RGB images for which the exit analyzer was kept fixed and the entry polarizer was rotated to two symmetrical positions close to the extinction condition (crossed Nicols). These images will be referred to as POL + θ and POL − θ, where θ is the rotation angle from extinction. Fig. 1b and c.

As crystal discrimination depends on the contrast between adjacent crystals, it also depends on the angle θ. Thus, five values of θ (±5°, ±10°, ±15°, ±20°, ±30°) were tested, and the results compared to search for an optimal value. Non symmetrical angular image pairs were also tested.

2.2. Image processing and analysis

2.2.1. Pre-processing

During image acquisition a displacement between BF and POL + θ/POL − θ images was detected. It probably occurs because polarizer/analyzer are mounted slightly oblique to the optical axis to avoid spurious reflections in the microscope. Although small, in the order of one pixel in the x and y directions, this misalignment created fake crystal boundaries. Thus, before any further processing, each triad of images was registered by an automatic routine through the traditional cross-correlation approach (Zitova and Flusser, 2003). The displacement increased with the angle θ, but was always automatically corrected by the routine.

2.2.2. Segmentation

The aim of segmentation is to distinguish the relevant components of the image. In the present case, these components are the individual hematite crystals. However, to reach this goal a novel approach was developed, comprising several steps.

1. *Segmentation of hematite regions*: The segmentation of hematite was carried out through intensity thresholding of the BF image. As hematite is much brighter than the other present phases, it is easy to select an intensity threshold from the image intensity histogram. The result is shown in Fig. 2a. The hematite binary image thereby obtained constitutes a mask that was used in the following image processing steps to remove any pixel outside the hematite phase.
2. *Coarse segmentation of hematite grains*: In this step a first detection of grain boundaries was attempted, to be refined later. The classical Canny (1986) edge detection method was applied individually to the lightness component of each POL image, and the obtained binary images were combined through the logical operation "or". The resulting edge image was then subtracted from the hematite image from step 1. The main limitation, at this point, was that the detected edges were many times incomplete and did not form closed boundaries around crystals. Moreover, edges between adjacent crystals with similar color were not always detected.
3. *Super-segmentation of hematite grains*: To complete missing or broken edges, a binary watershed technique was applied to the coarse segmented image from step 2. The inverted Euclidean Distance Transform was employed to process this image, and then the watershed segmentation (Beucher and Lantuéjoul, 1979) was applied. This procedure actually lead to a binary image in which the grains were separated, but many of them were strongly fragmented. The use of Euclidean Distance Transform in a binary watershed procedure can promote over-segmentation (Chen et al., 2004), which is desirable in the present case. See Fig. 2b.
4. *Generation of grain seeds*: Each grain fragment from the previous step went through an ultimate erosion (Serra, 1982) and was thus reduced to a single pixel seed. See Fig. 2c. These seeds were then used in a sequence of grain growing and merging, described in the following.
5. *Grain growing and merging*: A modified region growing method (Gomes et al., 2010) was applied to the seed image so that each seed grew back to a crystal. Because the seeds came from a super-segmented image, there must be a way to merge growing

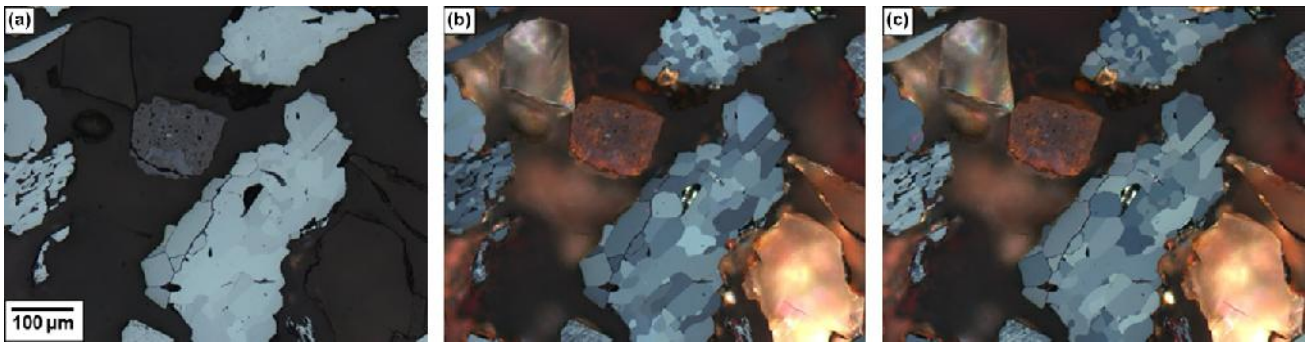

Fig. 1. (a) Bright field image; (b) polarization image 1 – polarizer angle = +10°; (c) polarization image 2 – polarizer angle = −10°.

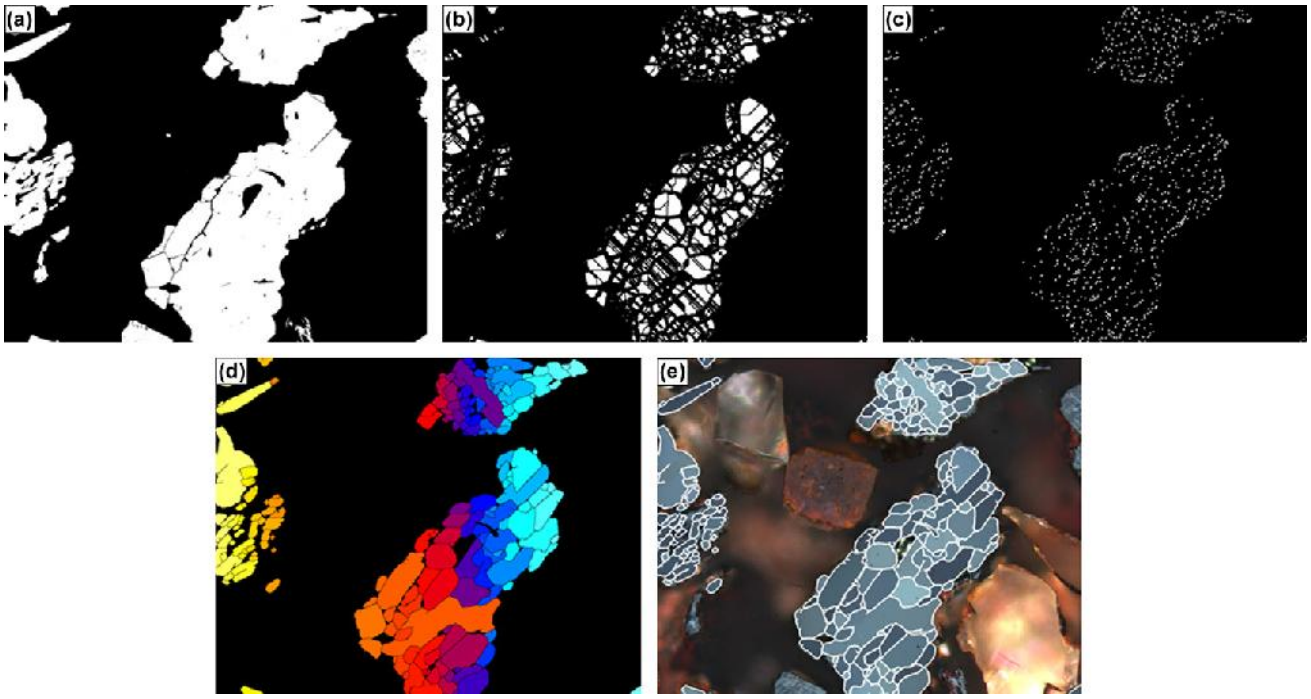

Fig. 2. (a) Discrimination of hematite regions; (b) super-segmentation of hematite grains; (c) grain seeds; (d) color coded reconstructed grains; (e) detected boundaries perimposed on POL image. (For interpretation of the references to color in this figure legend, the reader is referred to the web version of this article.)

regions that actually belonged to the same crystal. This was done combining the position information from the seeds image with the reflectance information from the pair of POL images. A typical result is shown color coded in Fig. 2d. The resulting reconstructed boundaries are shown in Fig. 2e, superimposed onto one of the POL images. As this step is the core of the crystal discrimination algorithm, it is described in detail in the following section.

2.3. Modified region growing algorithm

The region growing algorithm employed in this paper is quite different from the classical method of Adams and Bischof (1994). It is fed by both POL images as well and by the seeds image. A pixel connected to a grain is considered as belonging to it if its maximum Euclidean distance in RGB space from the corresponding seed pixel in the POL images is smaller than a fixed threshold. Specifically, a pixel $p(x, y)$ connected to a grain g that is defined by the seed pixel $p(x_g, y_g)$ pertains to the grain g only if the following rule is obeyed:

$$d^g(x,y) < t \tag{1}$$

where t is a threshold value that ranges between 0 and 1; and $d^g(x,y)$ is the maximum Euclidean distance in RGB space between the corresponding pixels of $p(x, y)$ and $p(x_g, y_g)$ in both POL images, computed as

$$d^g(x,y) = Max(d_1^g(x,y), d_2^g(x,y)) \tag{2}$$

$$d_i^g(x,y) = \sqrt{(R_i(x,y) - R_i(x_g,y_g))^2 + (G_i(x,y) - G_i(x_g,y_g))^2 + (B_i(x,y) - B_i(x_g,y_g))^2} \tag{3}$$

where i is 1 or 2, indicating POL image 1 or 2, respectively; $d_i^g(x,y)$ is the Euclidean distance in RGB space between the corresponding pixels of $p(x, y)$ and $p(x_g, y_g)$ in the POL image i; and $R_i(x, y)$, $G_i(x, y)$, $B_i(x, y)$ are the RGB values of the corresponding pixel $p(x, y)$ in the POL image i.

The region growing algorithm evolves finding grains automatically. At first, one grain is generated from each seed. The obtained grains are then combined through the logical operation "or". Thus, if two or more grains overlap, they are merged.

Table 1
Optimization data for the polarization angle θ.

Field	Manual grain count	θ (°)	Automatic grain count	Relative error (%)	t
1	189	5	138	27.0	0.027
		10	183	3.2	0.032
		15	174	7.9	0.035
		20	168	11.1	0.038
		30	160	15.3	0.040
2	325	5	251	22.8	
		10	315	3.1	
		15	298	8.3	
		20	275	15.4	
		30	269	17.2	
3	290	5	184	36.6	
		10	271	6.6	
		15	262	9.7	
		20	250	13.8	
		30	227	21.7	
4	325	5	232	28.6	
		10	308	5.2	
		15	257	20.9	
		20	235	27.7	
		30	170	47.7	
5	216	5	146	32.4	
		10	205	5.1	
		15	192	11.1	
		20	171	20.8	
		30	159	26.4	

If image brightness is normalized, $t = 0.023$ for all θ values.

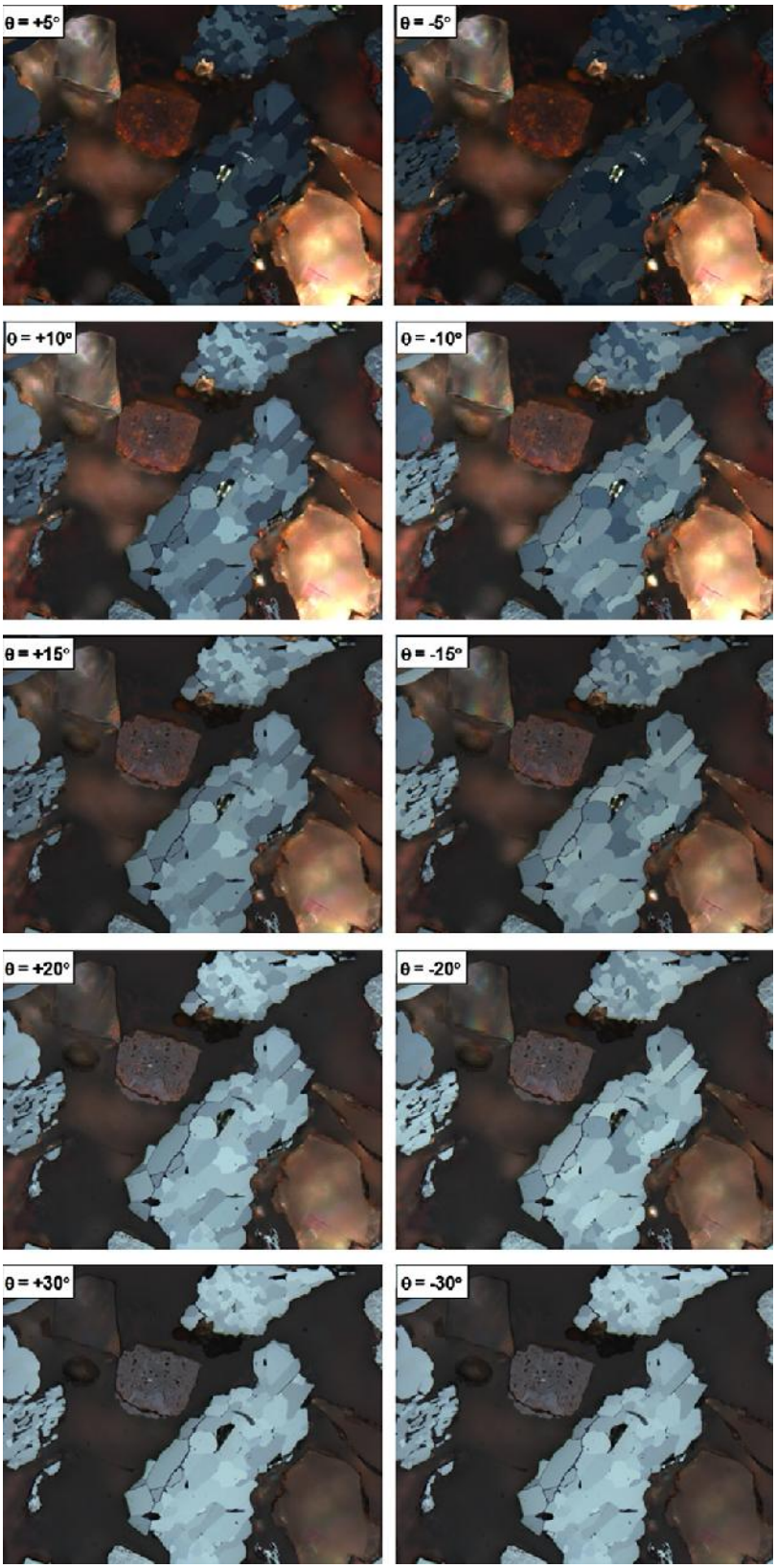

Fig. 3. Polarized image pairs for Field 1 and 5 polarization angles.

The only parameter to adjust is the threshold t. This threshold depends on the RGB intensities of the pixels in the POL images, which in turn depends on the polarization angle θ. Nevertheless, if image brightness is normalized, the parameter t can be fixed for all θ values.

2.2.4. Measurements, optimization and accuracy check

Since grain discrimination depends on both θ and t, the resulting images must be compared to determine the optimal values for these variables. For each value of θ, the best value of t was determined by visual comparison between the segmented image

and the original POL images. The best value of θ was then determined by comparing the number of grains obtained automatically with the result of a manual count by a skilled operator. Grain count by itself may be a misleading parameter, as a similar number of grains may be obtained even without a true correspondence between manually and automatically obtained grains. But a qualitative visual comparison also indicated an optimal situation for the angle determined by crystal count.

Once the optimal values of θ and t were determined the results were further checked by comparing the size and shape of obtained crystals against reference images. In the present work this was achieved by digital editing of the segmented image by a skilled operator while visually comparing to the original POL images. In this process false boundaries were deleted and missing boundaries were inserted.

The segmented and reference images were then automatically analyzed with a routine that measured crystal count, area (A), maximum and minimum Feret diameters (F_{max} and F_{min}) and Aspect Ratio ($AR = F_{min}/F_{max}$). Particles with $A < 25$ pixels^2 were discarded to reduce the influence of noise or spurious particles. The results were compared with the Student's t-test with 99% confidence level.

Results and discussion

Table 1 shows the optimization data for θ. For the 5 tested fields, the optimal value was always $\theta = 10°$, with a maximum relative error for grain count of 6.6%. The images shown in Figs. 1 and 2 correspond to Field 1 with $\theta = 10°$. The values of the threshold t for this field and the 5 polarization angles are also shown in Table 1. For the sake of visual comparison, Fig. 3 shows the 5 POL image pairs for Field 1.

During optimization it was also determined that non-symmetrical values of θ, or even two values of θ on the same side of the extinction point, led to worse results. It has occurred because the modified region growing method was designed regarding symmetrical angles. In practice, if non-symmetrical angles were employed, only the angle that leads to a greater image contrast was considered due to the maximization function (Eq. (2)) applied.

The best resulting images ($\theta = 10°$) were then edited as described above. The comparison data is shown in Table 2. For each field and each measurement parameter the minimum, maximum and mean values were obtained. Even though differences can be found between the automatically segmented and edited images, overall the results are very similar. From a statistical standpoint, there are no significant differences within a 99% confidence interval (99% CI), except for F_{min} in Field 4, and Aspect Ratio in Field 5.

The origin of these discrepancies can be traced back to specimen preparation defects. In Field 4 a scratch caused grain fragmentation in the automatically segmented image. During manual editing, this scratch was eliminated and grain fragments were merged. See Fig. 4. Fig. 5 shows the F_{min} distribution for segmented and edited images for Fields 1 and 4. While for Field 1 both distri-

ble 2
mparison between automatic and manually edited segmentation results.

Field	Parameter	Min		Max		Mean		≠ (99% CI)
		Auto	Edit	Auto	Edit	Auto	Edit	
1	Area (μm^2)	8.35	7.23	7270.84	7272.78	517.22	517.06	No
	F_{max} (μm)	4.5	4.54	207.88	207.88	32.23	33.12	No
	F_{min}(μm)	3.04	2.64	73.49	73.49	17.51	17.82	No
	AR	0.24	0.24	0.90	0.89	0.60	0.58	No
2	Area (μm^2)	8.9	8.35	83715.34	83715.34	1724.04	1700.36	No
	F_{max} (μm)	4.54	4.5	430.27	430.27	53.68	54.44	No
	F_{min}(μm)	2.81	2.64	272.19	272.19	28.69	28.99	No
	AR	0.15	0.09	0.92	0.92	0.58	0.57	No
3	Area (μm^2)	7.23	20.59	63545.94	63594.35	1838.47	2022.52	No
	F_{max} (μm)	4.02	6.52	502.07	393.51	54.30	62.55	No
	F_{min}(μm)	2.64	4.75	240.37	240.37	26.97	30.30	No
	AR	0.18	0.19	0.89	0.89	0.56	0.55	No
4	Area (μm^2)	7.79	22.82	39351.28	37895.72	1309.13	1561.48	No
	F_{max} (μm)	4.25	7.45	457.07	451.91	44.82	54.19	No
	F_{min}(μm)	2.64	4.75	143.12	143.12	24.97	30.19	Yes
	AR	0.19	0.21	0.94	0.94	0.60	0.60	No
5	Area (μm^2)	7.51	11.69	19340.48	18494.3	1408.73	1680.78	No
	F_{max} (μm)	3.84	5.97	295.76	290.96	47.26	58.01	No
	F_{min}(μm)	2.64	2.18	154.56	184.1	23.31	27.78	No
	AR	0.23	0.12	0.87	0.88	0.57	0.52	Yes

Auto – result from automatic segmentation. Edit – result from manually edited images. ≠ (99% CI) – statistical difference between Auto and Edit with 99% confidence interval.

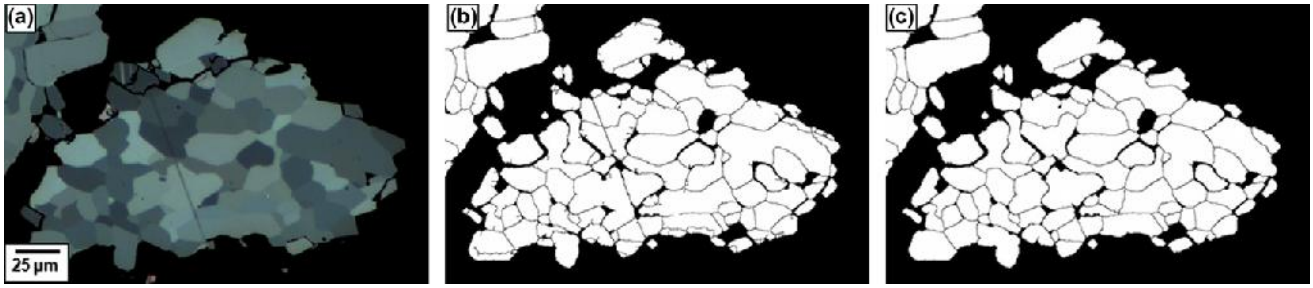

Fig. 4. (a) A small part of Field 4 showing a scratch; (b) result of automatic segmentation; (c) after manual editing.

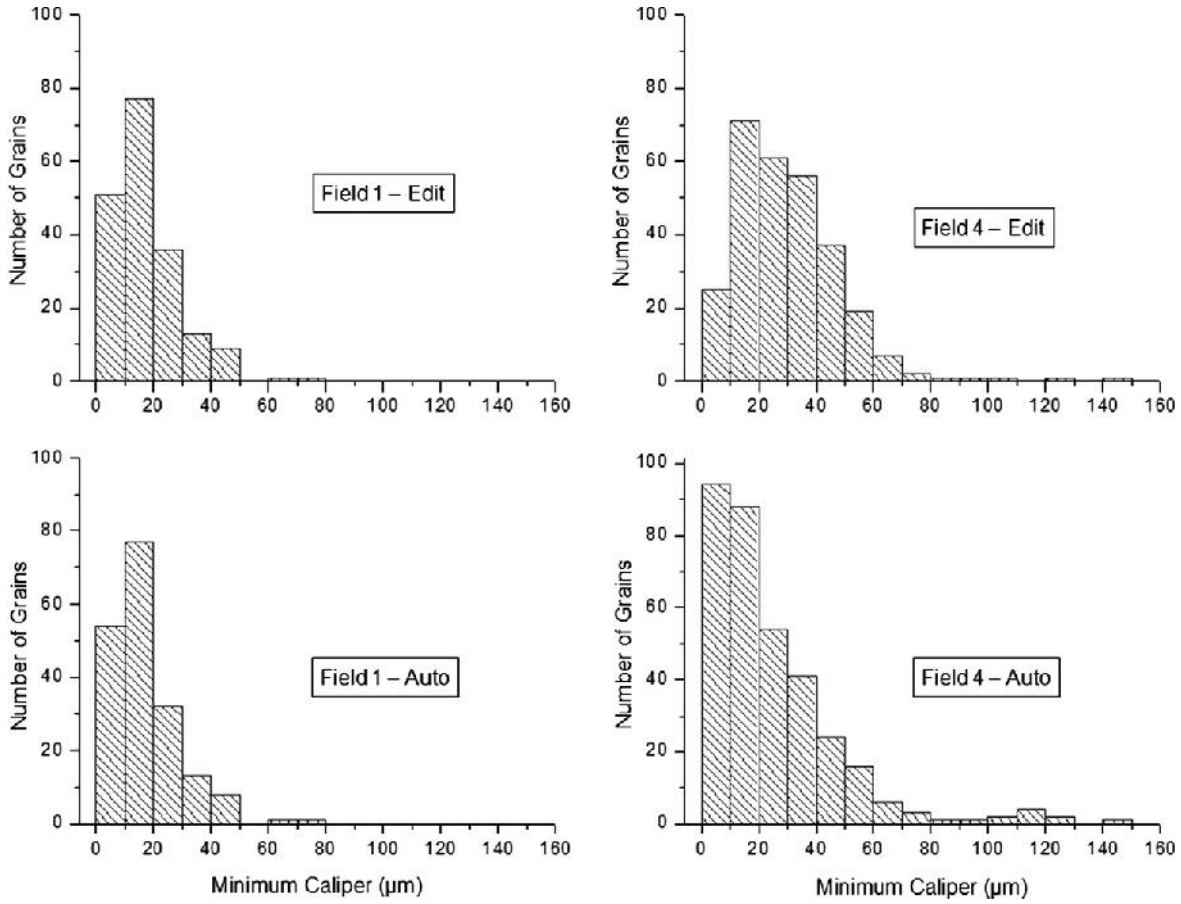

Fig. 5. Minimum caliper distribution for Fields 1 (left) and 4 (right) obtained from edited (top) and automatically segmented (bottom) images.

butions are very similar, for Field 4 there is a larger number of smaller objects. For this parameter, these differences affect the distribution significantly.

Even though not shown here, in Field 5 there were many false small grains created by the automatic segmentation at the outer edges of the hematite regions. This can be explained by contrast variations due to residual relief from specimen preparation, that is stronger exactly in the boundary between hematite and the mounting resin used.

It is important to mention that a one to one comparison between grains in segmented and edited images is not possible. Not only the number of grains is different, as discussed above, but the numbering sequence is also different as this is defined automatically by the image analysis routine when scanning the binary images to detect the grains.

4. Conclusions

A novel method for automatic discrimination of crystals employing polarized RLM was developed.

The method employs traditional image processing operations and proposes an optimized reflectance distance classifier to control region growing from automatically obtained seeds. It is worth mentioning that the proposed region growing procedure is very robust and is able to deal with the excessive number of seeds derived from the watershed segmentation.

The results are promising. The vast majority of grains were correctly identified. Even adjacent crystals with similar colors were discriminated. The method is essentially automatic once the images have been captured with an optimal polarization angle, which was found to be close to 10° for the tested samples. The only adjustable parameter is t, which controls the sensitivity of pixel Euclidean distance in RGB space.

However, some limitations must be pointed out. Given its discrimination capability, the method is also sensitive to problems in sample surface due to specimen preparation, such as scratches or relief. This only highlights the well-known requirement of excellent specimen preparation to allow automatic image analysis.

It is also important to mention that the image acquisition step may be labor intensive, as it requires three images per field (sample location), and tens to hundreds of fields are normally required to provide a representative sampling of the material. Although field scanning is motorized and computer controlled in the used microscope, polarizer rotation is manual. A filter wheel can be employed to provide polarizers in pre-defined angles. In fact, this arrangement can be useful for expert systems, but it is not a generic solution. As future work, the authors intend to motorize the polarizer rotation procedure.

Its application to hematite crystals in iron ore is a relevant step in ore quality control and opens the possibility of crystal size measurement and more sophisticated crystal morphology identification, which is currently under development. The goal is to choose shape parameters that allow the separation of hematite grains into pre-defined classes (lamellar, granular, recrystallized, etc.) identified by a skilled operator. Once a large number of grains has been measured and visually classified, this data can be used as a training set for a statistical classifier that will automatically identify the correct hematite class for both individual crystals and groups of crystals.

Acknowledgments

The support of CNPq and CAPES, Brazilian Agencies, and MCT is gratefully acknowledged. The fruitful discussions with Maria Beatriz Vieira from CTF/Vale were fundamental for the development of the present work. The help of Daisiana Brisola in image editing and measurement is also acknowledged.

References

Adams, R., Bischof, L., 1994. Seeded region growing. IEEE Transactions on Pattern Analysis and Machine Intelligence 16 (6), 641–647.

Beucher, S., Lantuéjoul, C., 1979. Use of watersheds in contour detection. In: Proceedings of International Workshop on Image Processing, Real-time Edge and Motion detection/estimation. CCETT/IRISA, Rennes, pp. 2.1–2.12.

Canny, J., 1986. A computational approach to edge detection. IEEE Transactions on Pattern Analysis and Machine Intelligence 8 (6), 679–698.

Chen, Q., Yang, X., Petriu, E.M., 2004. Watershed segmentation for binary images with different distance transforms. In: Proceedings of 3rd IEEE International Workshop on Haptic, Audio and Visual Environments and their Applications. IEEE, Piscataway, pp. 111–116.

Criddle, A.J., Stanley, C.J., 1993. Quantitative Data File for Ore Minerals, third ed. Chapman & Hall, London.

Donskoi, E., Suthers, S.P., Fradd, S.B., Young, J.M., Campbell, J.J., Raynlyn, T.D., Clout, J.M.F., 2007. Utilization of optical image analysis and automatic texture classification for iron ore particle characterization. Minerals Engineering 20, 461–471.

Gomes, O.D.M., Paciornik, S., 2008a. Iron ore quantitative characterization through reflected light-scanning electron co-site microscopy. In: Proceedings of Ninth International Congress on Applied Mineralogy. AusIMM, Carlton, pp. 699–702.

Gomes, O.D.M., Paciornik, S., 2008b. RLM-SEM co-site microscopy applied to iron ore characterization. In: Annals of 2nd International Symposium on Iron Ore. ABM, São Paulo, pp. 218-224.

Gomes, O.D.M., Paciornik, S., Alvarez, J.C., 2010. A simple methodology for identifying hematite grains under polarized reflected light microscopy. In: Proceedings of 17th International Conference on Systems, Signals and Image Processing – IWSSIP 2010. EdUFF, Niterói, pp. 428–431.

Gribble, C., Hall, A.J., 1992. Optical Mineralogy: Principles and Practice. UCL Press, London.

Pirard, E., Lebichot, S., 2004. Image analysis of iron oxides under the optical microscope. In: Applied Mineralogy: Developments in Science and Technology, vol. 1. ICAM-BR, São Paulo, pp. 153–156.

Pirard, E., Lebichot, S., Krier, W., 2007. Particle texture analysis using polarized light imaging and grey level intercepts. International Journal of Mineral Processing 84, 299–309.

Santos, L.D., Brandão, P.R.G., 2005. LM, SEM and EDS study of microstructure of Brazilian iron ores. Microscopy and Analysis 19, 17–19.

Serra, J., 1982. Image Analysis and Mathematical Morphology. Academic Press, London.

Vieira, C.B., Rosière, C.A., Pena, E.Q., Seshadri, V., Assis, P.S., 2003. Avaliação técnica de minérios de ferro para sinterização nas siderúrgicas e minerações brasileiras: uma análise crítica. Revista Escola de Minas 56, 97–102.

Zitova, B., Flusser, J., 2003. Image registration methods: a survey. Image and Vision Computing 21 (11), 977–1000.